computers

MDPI

Article

BICM-ID with Physical Layer Network Coding in TWR Free Space Optical Communication Links †

Alaa A. Saeed Al-Rubaie [1,*], Zina M. Hassan Abu Almaalie [2] and Zabih Ghassemlooy [2]

[1] Engineering Department, Directorate of Reconstruction and Projects, Ministry of Higher Education and Scientific Research, Street 52, Al-Rusafa, Baghdad 55509, Iraq

[2] Optical Communications Research Group, Faculty of Engineering and Environment, Northumbria University, Newcastle upon Tyne NE1 8ST, U.K.; zina.almaalie@northumbria.ac.uk (Z.M.H.A.A.); z.ghassemlooy@northumbria.ac.uk (Z.G.)

* Correspondence: alaa.sd1@gmail.com; Tel.: +44-07434839206

† This paper is an extended version of our paper published in the 8th Computer Science and Electronic Engineering (CEEC), Colchester, UK, 28–30 September 2016.

Received: 15 May 2017; Accepted: 18 July 2017; Published: 21 July 2017

Abstract: Physical layer network coding (PNC) is a promising technique to improve the network throughput in a two-way relay (TWR) channel for two users to exchange messages across a wireless network. The PNC technique incorporating a TWR channel is embraced by a free space optical (FSO) communication link for full utilization of network resources, namely TWR-FSO PNC. In this paper, bit interleaved coded modulation with iterative decoding (BICM-ID) is adopted to combat the deleterious effect of the turbulence channel by saving the message being transmitted to increase the reliability of the system. Moreover, based on this technique, comparative studies between end-to-end BICM-ID code, non-iterative convolutional coded and uncoded systems are carried out. Furthermore, this paper presents the extrinsic information transfer (ExIT) charts to evaluate the performance of BICM-ID code combined with the TWR-FSO PNC system. The simulation results show that the proposed scheme can achieve a significant bit error rate (BER) performance improvement through the introduction of an iterative process between a soft demapper and decoder. Similarly, Monte Carlo simulation results are provided to support the findings. Subsequently, the ExIT functions of the two receiver components are thoroughly analysed for a variety of parameters under the influence of a turbulence-induced channel fading, demonstrating the convergence behaviour of BICM-ID to enable the TWR-FSO PNC system, effectively mitigating the impact of the fading turbulence channel.

Keywords: physical layer network coding; free space optical communication; bit interleaved coded modulation with iterative decoding; turbulence-induced channel; Monte Carlo simulation; ExIT charts

1. Introduction

Although network coding has emerged as a new paradigm for communication to provide significantly increased network throughput [1], a valuable expansion technique introduced by [2] known as physical layer network coding (PNC) has an improved throughput for a two-way relay (TWR) network. A free space optical (FSO) communications link is an emerging broadband wireless access candidate, which has attracted significant attention for a variety of applications, such as a terrestrial FSO system in complementing the existing wireless radio frequency (RF) solution [3], for example, and utilizing the RF spectrum with cognitive radio networking enabling users to exploit femto base stations to improve the capacity performance [4]. The superior characteristics of the FSO technology are considered an advantage of the communication owing to the high security, cost-effectiveness, virtually unlimited bandwidth for achieving a very high aggregate capacity, simplicity of system design/setup, no licensing requirements for its utilization and reduced

interference [5]. However, atmospheric turbulence is a natural phenomenon commonly observed in terrestrial FSO systems, where the refractive index varies along the propagation path due to changes in atmospheric temperature, pressure and wind speed [6]. Furthermore, the weather condition was discussed in [7] to emphasize the importance of environmental conditions and atmospheric parameters. Therefore, laser beams propagating through the turbulent channel are highly susceptible to the adverse effects of turbulence-induced scintillation [8]. The concept of relay-assisted communications has recently been introduced in FSO systems to mitigate the degrading effects of the atmospheric turbulence and improve the system performance in the presence of the non-line-of-sight (NLOS) path between two FSO nodes in the network [9]. A number of analytical and simulation studies on the TWR-FSO system have been considered such as the amplify-and-forward (AF) schemes [10], decode-and-forward (DF) [11], linear network-coding at the relay node [12] and a recently-formed concept of buffer-aided relaying in [13]. For PNC demapping/mapping at the relay, the full utilization of TWR-FSO network resources was studied in [14]. Forward error correction (FEC) has been adopted for controlling errors in data transmission over a noisy communication channel to ensure a reliable communication system. The researcher in [15] utilized the packet-layer forward error correction to show its strength in a slow atmospheric fading channel and which affected the number of packet losses. Recently, the performance of end-to-end (E2E) convolutional code combined with TWR-FSO PNC was implemented by [16]. K. Kumar et al. in [17,18] described the bit interleaved coded modulation with iterative decoding (BICM-ID) code detection in parallel FSO and RF links. The powerful FEC is BICM-ID [19], where BICM-ID is applied as an iterative channel coding method in the TWR-FSO PNC system to minimize the degrading effects of the FSO channels and to increase the robustness of a system against the noise and the interference. The effects of turbulence-induced channel fading under a clear weather condition is also considered. The result reveals that the TWR-FSO PNC scheme can employ an iterative decoding means to achieve improved performance in terms of bit error rate (BER). However, extrinsic information transfer (ExIT) charts are given as an advanced technique in a precise manner for describing the convergence behaviour of the iterative decoding method [20]. Therefore, ExIT charts are involved to investigate the achievable convergence for the E2E BICM-ID TWR-FSO PNC scheme. The rest of this paper is organized as follows: Section 2 presents the system description. Section 3 introduces the ExIT charts analysis, and Section 4 illustrates the simulation results. Finally, Section 5 contains the conclusion.

2. System Description

2.1. PNC Model

The system is a TWR channel with PNC located in the relay that allows two users to exchange messages in a wireless network. PNC consists of three nodes: User-1, User-2 and a relay, as depicted in Figure 1. Each user has one transmitter aperture, while the relay has two directional antennas. There is no direct link between User-1 and User-2. Therefore, the relay node is used to establish a communication link for the users in two phases: multiple access (MAC) phase (first time slot), which dedicates the entire transmit node to the relay, and broadcast (BC) phase (second time slot), which dedicates the entire broadcast relay node to the users. We assume that the two user nodes operate over a half-duplex link with the same transmit power and perfect synchronization. During the MAC phase, User-1 and User-2 transmit the information bearing signals S_1 and S_2 to the relay node over their respective links. At the relay, the received signal $R = S_1 + S_2 + W$ is mapped by a special demapping/mapping technique to produce a network-coded bit, Y, as $PNC : R \rightarrow Y$, where W represents the noise source. In the BC phase, the relay node broadcasts Y to both nodes over the corresponding link. At the respective destinations, the received signal $Y + W$ is recovered by an exclusive-OR (XOR) operation $\oplus$. The desirable information for User-1 and User-2 is $\hat{b}_2$ as $(Y + W) \oplus b_1 \rightarrow \hat{b}_2$ and $\hat{b}_1$ as $(Y + W) \oplus b_2 \rightarrow \hat{b}_1$, respectively.

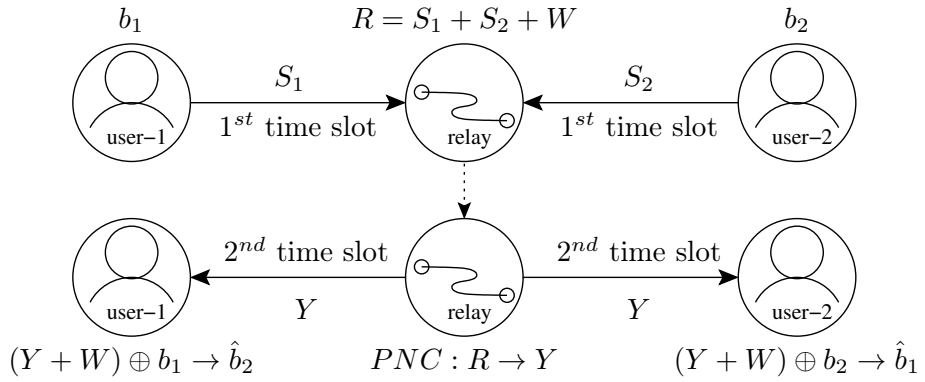

Figure 1. System model for two-way relay (TWR) with physical layer network coding (PNC).

2.2. Channel Model

For each node, the channel state h can be expressed as shown in [6] by:

$$h_k = h_s h_e h_l, \tag{1}$$

where k is the number of users, h_s is a random variable representing the intensity fluctuation due to the atmospheric turbulence, h_e is the misalignment fading due to the pointing error loss and h_l is the channel loss coefficient.

2.2.1. Atmospheric Turbulence-Induced Fading

Turbulence-induced signal fading is one of the main impairments affecting the operation of FSO systems. The distribution of the light intensity fading due to the weak turbulence can be described by a log-normal distribution as:

$$p(h_s) = \frac{\exp\left(\frac{(\ln(h_s) + \sigma_I^2/2)^2}{2\sigma_I^2}\right)}{\sqrt{2\pi\sigma_I^2 h_s}}, \tag{2}$$

where σ_I^2 is the scintillation index. For a weak turbulence regime, σ_I^2 is found to be proportional to Rytov variance σ_R^2, which can be calculated as shown in [3] by:

$$\sigma_R = \sqrt{1.23 \left(\frac{2\pi}{\lambda}\right)^{7/6} C_n^2 \, L_d^{11/6}}, \tag{3}$$

where λ is the wavelength and L_d is the link distance between the transmitter and receiver points. Typically, the refractive index range value of C_n^2 is from 10^{-12} meters$^{-2/3}$ (m$^{-2/3}$) for strong turbulence to 10^{-17} m$^{-2/3}$ for weak turbulence. However, the gamma-gamma distribution is utilized to address both the large- and small-scale scintillations under moderate-to-strong scenarios, which can be written as:

$$p(h_s) = \frac{2(\alpha\beta)^{\frac{\alpha+\beta}{2}} \, h_s^{\frac{\alpha+\beta}{2}-1} \, K_{\alpha-\beta}\left(2\sqrt{\alpha\,\beta\,h_s}\right)}{\Gamma(\alpha)\,\Gamma(\beta)}, \tag{4}$$

where $\Gamma(.)$ is the gamma function and $K_{\alpha-\beta}(.)$ is the modified Bessel function of the second kind of order $\alpha - \beta$. Parameters α and β represent the effective number of large-scale and small-scale turbulence eddies, respectively. If the optical radiation at the receiver is assumed to be a plane wave,

then the two parameters α and β that characterize the irradiance fluctuation distribution are related to the atmospheric conditions by:

$$\alpha = \left(\exp\left(\frac{0.49\ \sigma_R^2}{\left(1 + 1.11\ \sigma_R^{12/5}\right)^{7/6}} \right) \right)^{-1} \tag{5}$$

$$\beta = \left(\exp\left(\frac{0.51\ \sigma_R^2}{\left(1 + 0.69\ \sigma_R^{12/5}\right)^{7/6}} \right) \right)^{-1} \tag{6}$$

2.2.2. Pointing Errors

The model assumes a circular detection aperture of radius ω and a Gaussian spatial intensity profile of a beam waist radius on the received plane. The misalignment-fading model derived in [21] offers a tractable probability density function (pdf) for describing the behaviour of the pointing error loss, which takes into account the detector size, beam width and jitter variance as:

$$h_e = A_0 \exp\left(\frac{-2r_d^2}{w_b^2}\right), \tag{7}$$

where r_d is the radial displacement between the beam and the detector centre. The symbol of A_0 is the fraction of received power at a zero radial distance, which can be expressed as:

$$A_0 = \left(\mathrm{erf}(v_p)\right)^2, \tag{8}$$

where $\mathrm{erf}(.)$ denotes the error function and v_p can be defined as:

$$v_p = \sqrt{\pi/2}\frac{\omega}{w_L}, \tag{9}$$

where w_L is the beam waist radius and the term of $\frac{w_L}{\omega}$ is identified as the beam waist normalized by the radius ω of the receiver aperture. The w_b term represents the equivalent beam waist, which can be determined as:

$$w_b^2 = \frac{\sqrt{\pi} w_L^2 \mathrm{erf}(v_p)}{2 v_p \exp(-v_p^2)}. \tag{10}$$

2.2.3. Atmospheric Loss

The atmospheric channel attenuates the signal traversing it as a result of absorption and scattering processes, which can be described by the exponential Beers–Lambert law [22] as:

$$h_l = \exp(-\delta L_d), \tag{11}$$

where δ is the weather attenuation coefficient, which can be determined from the visibility data through Kim's model [23] as:

$$\delta = \left(\frac{3.91}{V}\right)\left(\frac{\lambda}{550}\right)^{-q}, \tag{12}$$

where V in kilometres (km) represents the visibility and q is the particle size distribution coefficient, which can be defined from [24] as:

$$q = \begin{cases} 1.6, & V > 50 \text{ km} \\ 1.3, & 6 \text{ km} < V < 50 \text{ km} \\ 0.16 + 0.34, & 1 \text{ km} < V < 6 \text{ km} \\ V - 0.5, & 0.5 \text{ km} < V < 1 \text{ km} \\ 0, & V < 0.5 \text{ km} \end{cases}. \tag{13}$$

2.3. System Model

In the relaying network structure with binary data transmission, the transmitter sends only one of two possible signals during each bit interval T_b. The encoder structure for a system employing BICM-ID is realized by a serial concatenation of the convolutional encoder, pseudo-random interleaver and mapper [19], as depicted in Figure 2. However, the mapper can be considered as a code due to M-bits being associated with each symbol, where M is defined as the constellation size of the utilized modulation scheme.

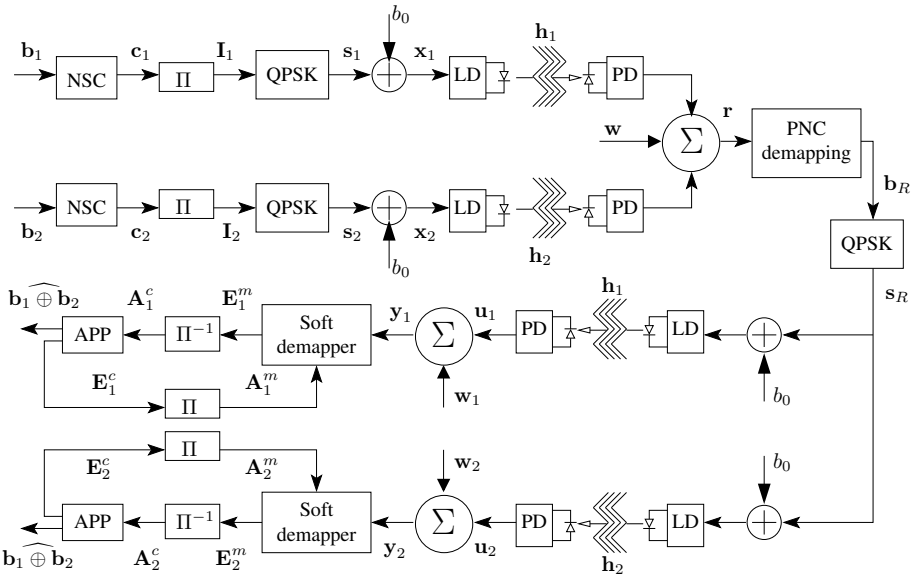

Figure 2. Block diagram for bit interleaved coded modulation with iterative decoding (BICM-ID) TWR-free space optical (FSO) with PNC. NSC, non-systematic convolutional; APP, a posteriori probability.

2.3.1. Transmitter

The information bit $[\mathbf{b}_k]_{n=0}^{N-1} \in GF(2)$ of length n is encoded by non-systematic convolutional (NSC) encoder to produce codeword bits $\mathbf{c}_k$ of length n/R_c, where R_c is the code rate. The sequence of code bit $\mathbf{c}_k$ is permuted by a bit-level interleaver, Π, to obtain $\mathbf{I}_k$ of length n/R_c. The M-ary mapping scheme groups $\log_2 M$ bits into each constellation point. Quadrature phase shift keying (QPSK) is adopted in this work, in which case we have four symbols representing the $\mathbf{s}_k$ sequence. To ensure that the optical modulated signals are all positive, a direct current (DC) bias level b_0 is added to the QPSK signal prior to intensity modulation (IM) of the light source, which can be expressed as:

$$\mathbf{x}_k = P_t[1 + \psi\, \mathbf{s}_k], \tag{14}$$

where P_t is the average transmit optical power and ψ is the modulation index satisfying the condition $-1 \leq \psi\, \mathbf{s}_k \leq +1$ in order to avoid clipping due to the over-modulation.

2.3.2. Relay

The relay received signal can be expressed as:

$$\mathbf{r} = R_s \sum_{k=1}^{K} h_k \mathbf{x}_k + \mathbf{w}, \tag{15}$$

where R_s is the responsivity of the detector, $\mathbf{x}_k$ is the optical signal intensity and h_k is the channel state. The $\mathbf{w}$ term is modelled as additive white Gaussian noise with zero mean and variance $\sigma^2 = N_0/2$, where $N_0/2$ is the two-sided noise power spectral density. The relay performs PNC demapping/mapping on the received $\mathbf{r}$ signal. However, in PNC, the relay node does not need to know the individual bits of the four unknowns within QPSK. Instead, it only needs to derive the demapping form $\mathbf{b}_R$ on the received symbols, which consists of two bits to produce the PNC mapping $\mathbf{s}_R$. The common approach for the relay demapping and then mapping of the synchronization algorithms embodies the application of a maximum likelihood (ML) criterion [25].

2.3.3. Receiver

At the receiver, we have adopted a soft-in-soft-out (SISO) to compute the log-likelihood ratio (LLR) of the information. The data detection algorithm mainly consists of a soft demapper, which provides the bit metric to the detector. The concept of the system depends on the demapper taking soft values $\mathbf{y}_k$ from the channel output and producing extrinsic information $\mathbf{E}_k^m$, which is passed through a bit deinterleaver to become a priori decoder input $\mathbf{A}_k^c$. The decoder's extrinsic information of the coded bits $\mathbf{E}_k^c$ is fed back to the demapper as a priori knowledge $\mathbf{A}_k^m$ through the bit interleaver, reducing the BER further in subsequent iterative processes.

3. ExIT Charts Analysis

The ExIT charts have become an essential part of iterative error correction code design and have also been used as a complementary design tool for traditional BER simulations. The method of bitwise mutual information was implemented as a tool for studying the convergence behaviour of iterative decoding schemes. The ExIT chart technique relies on the Gaussian approximation [26], but provides some intuition regarding the dynamics and convergence properties of an iteratively decoded code. The formulation of a turbo-cliff after a certain number of iterations enables us to predict a low BER for the ratio between the energy per information bit (E_b) and the variance of noise (N_0), E_b/N_0, in excess of the turbo-cliff. Therefore, the ExIT characteristics of the constituent decoders describe the processing of mutual information, which measures the dependence between two variables, associated with a priori information inputs to mutual information associated with the extrinsic information outputs. The mutual information I between the two variables can be expressed from [27] as:

$$I(X;L) = \frac{1}{2} \sum_{x \in \{0,1\}} \int_{-\infty}^{+\infty} Pr(\xi|x) \log_2 \left(\frac{2Pr(\xi|x)}{Pr(\xi|x=1) + Pr(\xi|x=0)} \right) d\xi, \tag{16}$$

where X is the information of finite size being fed through the input and $\mathbf{L}$ is the information produced in terms of the LLR with realization ξ. However, the property of symmetry is valid for any linear code decoded by using a posteriori probability (APP)-based decoders [28]. Likewise, the property of consistency is satisfied with the accurate computation of the LLR output [29]. Consequently, the properties of symmetry and consistency integration are closely approximated by using a time average to define the mutual information based on the demapper or the decoder component as:

$$I(X;L) \approx 1 - \frac{1}{N} \sum_{n=1}^{N} \log_2 \left(1 + e^{-\left(L_n[x_n] \right)} \right), \tag{17}$$

where N is the total number of observed L_n of LLRs. Additionally, the mutual information from the QPSK received decision symbol $\mathbf{L}$ can be calculated from [30] as:

$$I(X,L) = \frac{1}{M}\sum_{i=0}^{M-1}\mathbb{E}_{\xi|x_i}\left[\log_2\left(\frac{M}{1+e^{\Lambda_{x_i}[L]}}\right)\right], \tag{18}$$

where M states the bit per mapped codeword and $\mathbb{E}$ means expectation over $\{X, L\}$. Assuming equal transmission probabilities for all modulation symbols, the LLR Λ at M states of modulation symbols can be determined as:

$$\Lambda_{x_i}[L] = \ln\left(\frac{Pr(x_i|L)}{\sum_{j=1;j\neq i}^{M} Pr(x_j|L)}\right) \tag{19a}$$

$$= \ln\left(\frac{e^{-\ell_i/\sigma^2}}{\sum_{j=1;j\neq i}^{M} e^{-\ell_j/\sigma^2}}\right). \tag{19b}$$

where ℓ is the distance from receiving variable L to the symbol transmitted X.

Setup ExIT Function

The BICM-ID code is constructed from a serial arrangement of inner and outer codes. At the receiver, there is an iterative process between the inner code, the demapper D_m and the outer code, forming the decoder D_c to improve the link performance. However, the receiver for each constituent code is an SISO module, and the conditional pdf of the input LLRs to the SISO module is not known. Hence, the ExIT function setup for the BICM-ID system is simulated for the demapper and the decoder separately. Firstly, we investigate the transfer characteristic for the inner demapper, where the users' symbols are summed following QPSK mapping and then transmitted over the FSO link. The noisy signal $\mathbf{r}$ is captured by the PNC demapping scheme to generate the bit sequence $\mathbf{b}_R$ as can be observed in Figure 3.

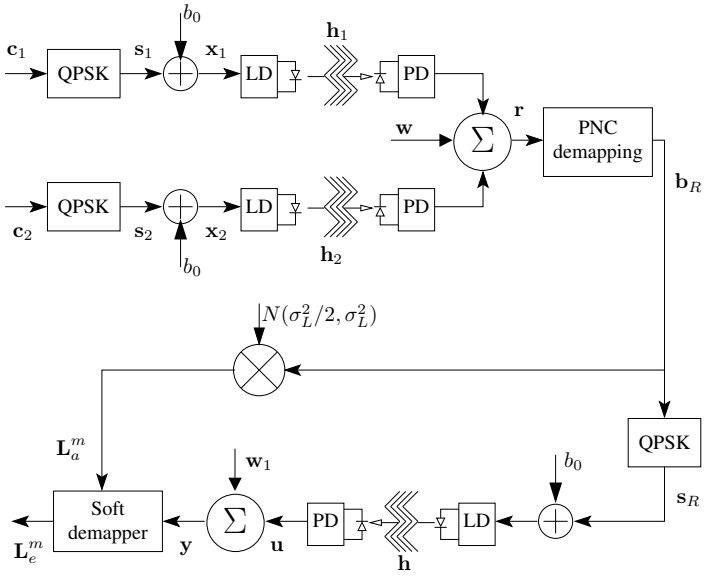

Figure 3. The demapper setup for TWR-FSO PNC system employing BICM-ID code to generate the ExIT function.

The bit sequence produced from the PNC demapping is multiplied by the independent samples taken from a Gaussian distribution with mean value $\sigma_L^2/2$ and variance σ_L^2 forming a priori information $\mathbf{L}_a^m$. Terms $\mathbf{L}_a^m$ and $\mathbf{y}$ are applied to the soft demapper, which has a transfer characteristic $I_{(E,\,D_m)}$ of:

$$I_{(E,\,D_m)} = \mathcal{T}_I(I_{(A,\,D_m)},\ E_b/N_0), \tag{20}$$

where $I_{(A,\, D_m)}$ is the mutual information between transmitted sequence and a priori LLR. Hence, the inner demapper system is affected by the channel information as it depends on E_b/N_0 caused by the LLR of $\mathbf{L}_a^m$ and $\mathbf{y}$, whereas the SISO decoder of PNC with BICM-ID starts with a block of independent message bits $\mathbf{b}_k$ from each user and is encoded by an NSC encoder to obtain $\mathbf{c}_k$. The outer decoder system setup is shown in Figure 4. The modulo-two sum code bits of users is represented by $\mathbf{c}$, which are modelled as random independent Gaussian distributed variables with a mean value of $\sigma_L^2/2$ and a variance of σ_L^2 to form the decoder input in terms of LLRs, $\mathbf{L}_a^c$ [31]. The decoder employs the maximum a posteriori algorithm in the logarithm domain (Log-MAP) to provide information about the source bits. Therefore, the decoder input is a priori information coming from the decoders $\mathbf{L}_a^c$ in terms of LLRs, where the outputs are extrinsic information of coded bits $\mathbf{L}_e^c$, which are in turn fed back for the next iteration, and with the $\mathbf{b}_1 \widehat{\oplus} \mathbf{b}_2$ operation to estimate source bits. Consequently, the decoder transfer characteristic $I_{(E,\, D_c)}$ is the transfer function of a priori mutual information $I_{(A,\, D_c)}$, which can be written as:

$$I_{(E,\, D_c)} = \mathcal{T}_I(I_{(A,\, D_c)}). \tag{21}$$

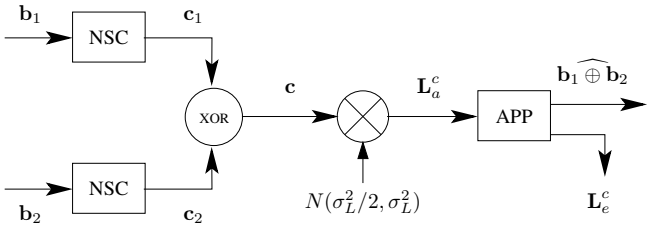

Figure 4. The decoder setup for TWR-FSO PNC system employing BICM-ID code to generate the ExIT function.

4. Simulation Results

The performance for the TWR-FSO PNC system with iterative decoding using the E2E BICM-ID code is performed over atmospheric turbulence fading channels ranging from weak to strong. Furthermore, an evaluation of the link performance is investigated by ExIT charts, taking into account the influence of channel impairments such as path loss, atmospheric turbulence fading and pointing errors. The investigation of the E2E coded TWR-FSO PNC system with iterative decoders depends on the mutual information between the transmitter and the receiver. Thus, the convergence behaviour of the proposed detectors of TWR network from the unknown received signal is evaluated.

4.1. Iterative Process

The transmitted source of data bits is encoded with a rate R_c 0.5 NSC encoder of a constraint length of five and generator polynomials of $[23\ 35]_8$. Consider that L_d is two kilometres (km); V in a clear weather condition is 10 km; λ is 1550 nanometres (nm); and R_s is one ampere per watt (A/W). For weak and strong turbulence, σ_R^2 and C_n^2 are 0.5, 1.6 and 0.75×10^{-14} m$^{-2/3}$, 1.00×10^{-13} m$^{-2/3}$, respectively. The encoded bits are anti-Gray mapped to a QPSK constellation. Figures 5 and 6 show the BER performance of BICM-ID with PNC over a log-normal (weak) and a gamma-gamma (strong) channels for various numbers of decoder iterations, respectively. As can be seen from the figures, the BER performance has to have the same behaviour after Iteration Number 2. In order to confirm the accuracy and usefulness of the system, the Monte Carlo method is adopted. Specifically, in Figures 7 and 8, we get the results of the BICM-ID TWR-FSO PNC system under weak and strong turbulence conditions. This is mainly due to the fact that the system under the strong turbulence model causes a degradation in the error performance. Consequently, the TWR-FSO with PNC can be compared with the log-normal and the gamma-gamma channels in terms of uncoded, system employed E2E non-iterative code as the convolutional code and the system employing E2E BICM-ID code, as shown in Figures 9 and 10 for a log-normal and a gamma-gamma channel model, respectively. Hence, for

weak and strong turbulence fading channels, we observe that the BER performance of the proposed system with BICM-ID outperforms the uncoded and non-iterative convolutional code systems. As we can see in Figure 9, the system with BICM-ID shows an improvement when adopting iterative demapping and decoding. For instance, there is an improvement of about 12 dB of E_b/N_0 at a BER of 10^{-4} for the proposed system compared to that of uncoded as distinguished for weak turbulence. Whereas for a system with a convolutional code, the improvement is approximately 6 dB of E_b/N_0 at a BER of 10^{-4}. However, for the systems in Figure 10 with BICM-ID, the BER improves slightly for the iterative demapping and decoding. For example, at a BER of 10^{-2}, the E_b/N_0 difference is about 8 dB for the proposed system compared to that of uncoded TWR-FSO PNC system. At a BER of 10^{-4}, the E_b/N_0 for the system with convolutional code is 40 dB and for system with BICM-ID code is about 37.5 dB. Therefore, the effects of iterative decoding are detected within an atmospheric turbulence fading channel. Nevertheless, the results show that BICM-ID codes with trellis-based decoding algorithms are suited to TWR-FSO PNC networks. This is mainly because in an atmospheric turbulence fading channel, introducing the interleaver produces a higher degree of diversity order and therefore guarantees significant improvement.

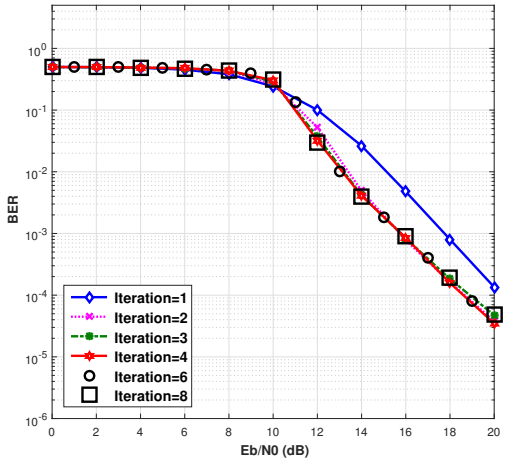

Figure 5. BER performance of BICM-ID with PNC over a log-normal channel for various numbers of decoder iterations.

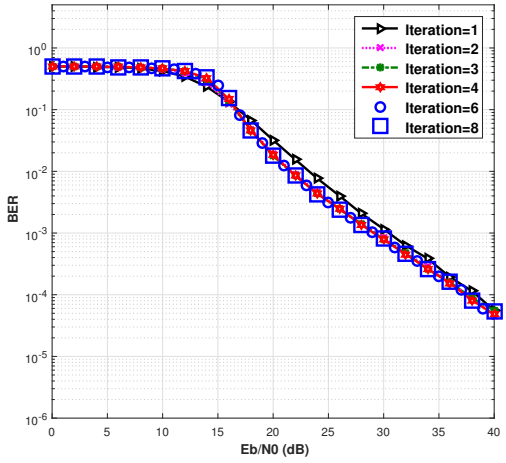

Figure 6. BER performance of BICM-ID with PNC over a gamma-gamma channel for various numbers of decoder iterations.

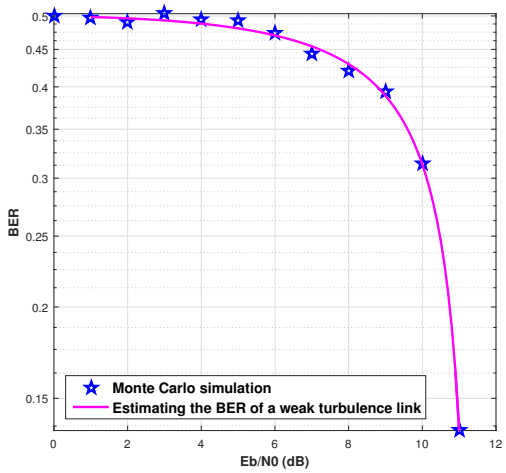

Figure 7. Monte Carlo method applied to the BICM-ID TWR-FSO with PNC system over a weak turbulence link.

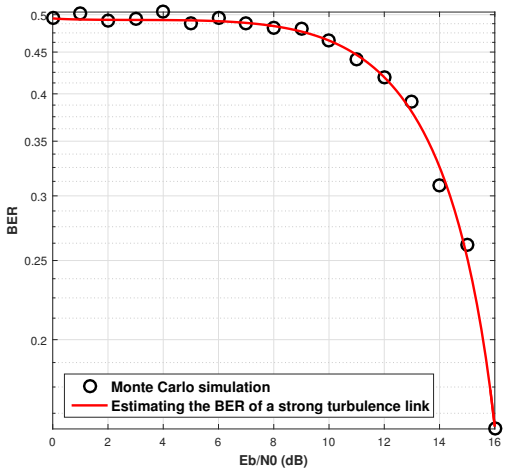

Figure 8. Monte Carlo method applied to the BICM-ID TWR-FSO with PNC system over a strong turbulence link.

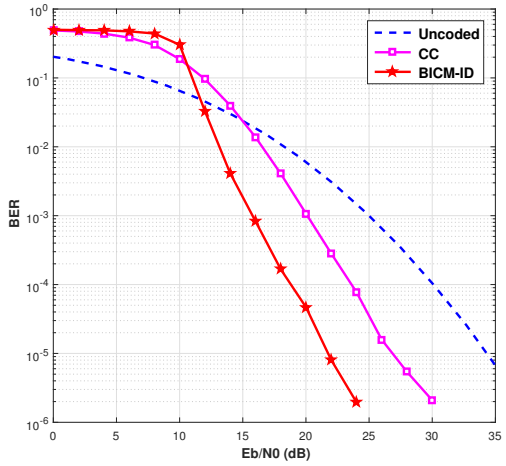

Figure 9. BER performance of TWR-FSO with PNC over a log-normal channel when employing uncoded, E2E convolutional code and E2E BICM-ID codes.

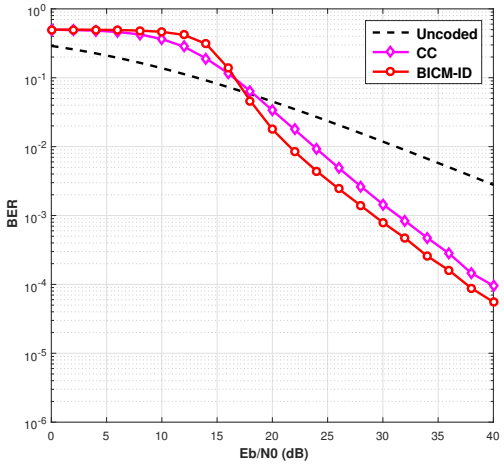

Figure 10. BER performance of TWR-FSO with PNC over the gamma-gamma channel when employing uncoded, E2E convolutional code and E2E BICM-ID codes.

4.2. Convergence Behaviour

At the commencement of the BICM iterative decoding process, the TWR-FSO PNC systems were presented as the ExIT function. The main idea when utilizing the ExIT chart is to track the pdf of information messages that are exchanged in the iterative decoding process, where the decoder uses the Bahl—Cocke—Jelinek—Raviv (BCJR) algorithm. Furthermore, links have been made between ExIT charts and the corresponding BER curves. The ExIT chart provides an accurate prediction of the convergence behaviour, which is verified and visualized by the simulated decoding trajectory. Consequently, ExIT charts visualize the density evolution of the extrinsic LLRs over the iterations using a single parameter of the average mutual information between the coded bits at the transmitter and the LLRs at the receiver. To predict the evolution of the investigated parameter, each SISO receiver component has close to ideal a priori information from the other receiver components. To evaluate and optimize the convergence behaviour of iterative receivers, a number of blocks is simulated for different values of σ^2 in order to estimate the output mutual information for the decoder. When natural (anti-Gray) mapping is utilized in the transfer function of the demapper, the demapper is affected by log-normal and gamma-gamma channel models as it depends on the SNR in terms of E_b/N_0. Therefore, the demapper transfer characteristics almost approach non-convex shapes depending on the SNR values. Figure 11 shows the ExIT chart function when the channel is log-normal for 0, 2, 4 and 6 dB of SNR values, whereas Figure 12 shows the ExIT chart function when the channel is gamma-gamma for 0, 2, 4, 6 and 8 dB of SNR values. Observing that the transfer characteristic has a steep slope, it can be seen that it yields a strong potential for performance improvement in the PNC with BICM-ID system. Moreover, a decrease/increase in the value of SNR will shift the ExIT curve down/up, respectfully. The ExIT function of the outer code is depicted in Figure 13, which shows the transfer characteristics of code specification. For example, the stronger code of a constraint length of nine has a steeper ExIT function than the weaker code of a constraint length of three and therefore needs lower mutual information at the input to produce high quality LLRs at the output. Furthermore, the decoder curve shows the relationship between the a priori information and predicts the BER for the system by using the ExIT function, as shown in Figure 14. As part of the research to assess the effectiveness of the BICM-ID TWR-FSO PNC system, we can observe that the simulation results along with the Monte Carlo simulation match with the exact analytical results of the ExIT charts. However, the system with the strong turbulence condition affects the convergence behaviour more than the weak turbulence condition. Therefore, we evaluated the I_E with respect to the range of SNR by Monte Carlo simulation based on the demapper TWR-FSO PNC system under the weak and strong turbulence model. More specifically, in Figures 15 and 16, there is a one-to-one correspondence between SNR and I_E in the demapper TWR-FSO PNC system. The relationship between the mutual information

and the variance of LLRs was formally described in [27]. With an increase in SNR, we increase the knowledge of information in the mutual information of I_E. Therefore, the trajectory of the iteration system is evaluated by the progress of the data components in terms of mutual information, and both characteristic functions can be plotted in a single figure. Consequently, in the graph, the convergence of curves for the system gives the approaches between the demapper and the inverted ExIT function of the decoder. Hence, the trajectory of the system can be predicted as the stair case between the two curves of the demapper and decoder. For the trajectory to propagate, the increase in the SNR value must raise the transfer characteristic of the demapper high enough to open the tunnel. The system with the log-normal channel model in Figure 17 shows that the trajectory that encountered the tunnel opening closes at $I_{(A;\,E,\,D_c)}$= 0.92 and $I_{(E,\,D_m;\,A)}$= 0.68 for SNR = 8 dB and at SNR = 10 dB. The tunnel closes at $I_{(A;\,E,\,D_c)}$= 0.98 and $I_{(E,\,D_m;\,A)}$= 0.78, implying that the receiver will not converge at 8 and 10 dB, whereas the tunnel opens at SNR = 11 dB, and the trajectory experiences a bottleneck at $I_{(A;\,E,\,D_c)}$ = 1 and $I_{(E,\,D_m;\,A)}$ = 0.82, implying that a further increase in iterations at this particular value of SNR will not improve the performance of the system. Again, for the system with gamma-gamma in Figure 18, it can be seen that the tunnel opening closes at $I_{(A;\,E,\,D_c)}$= 0.09 and $I_{(E,\,D_m;\,A)}$= 0.34 for SNR = 10 dB, implying that the receiver will not converge. There is a similar situation for SNR = 12 dB with $I_{(A;\,E,\,D_c)}$= 0.75 and $I_{(E,\,D_m;\,A)}$= 0.56, SNR = 14 dB with $I_{(A;\,E,\,D_c)}$= 0.96 and $I_{(E,\,D_m;\,A)}$= 0.7 and, finally, SNR = 15 dB at $I_{(A;\,E,\,D_c)}$= 0.98 and $I_{(E,\,D_m;\,A)}$= 0.75. As the iteration continues, the iterative decoder converges to a final point at the intersection of the ExIT chart curves. Hence, the mutual information improves by following the guide of the tunnel between curves, and the convergence occurs at SNR = 16 dB for the proposed system with the strong channel at $I_{(A;\,E,\,D_c)}$= 1 and $I_{(E,\,D_m;\,A)}$= 0.8. Consequently, the ExIT chart provides an accurate prediction of the convergence behaviour, which is verified and visualized by the simulated decoding trajectory.

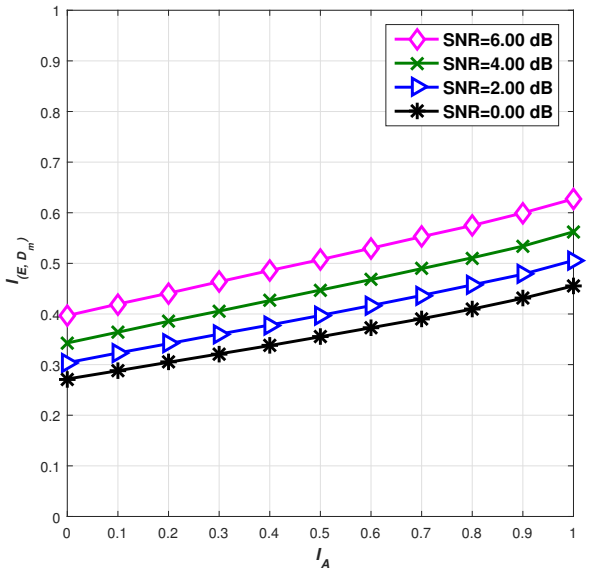

Figure 11. ExIT chart function for the demapper PNC system employing the TWR-FSO log-normal channel model.

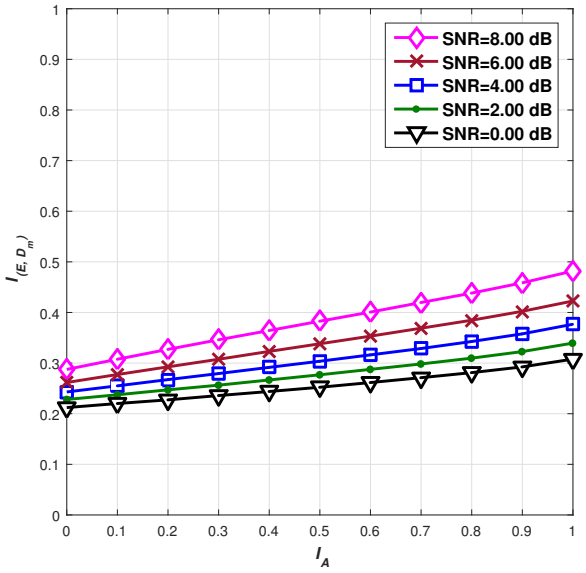

Figure 12. ExIT chart function for the demapper PNC system employing the TWR-FSO gamma-gamma channel model.

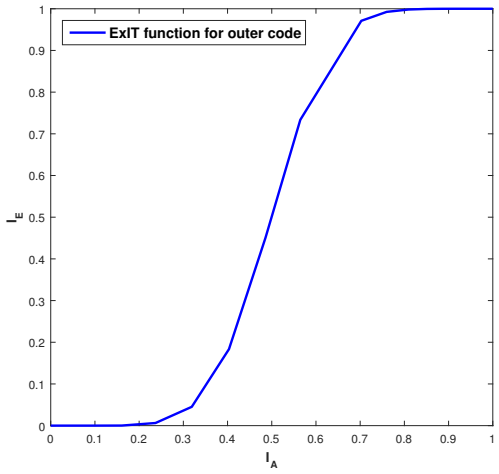

Figure 13. ExIT chart function for the outer decoder.

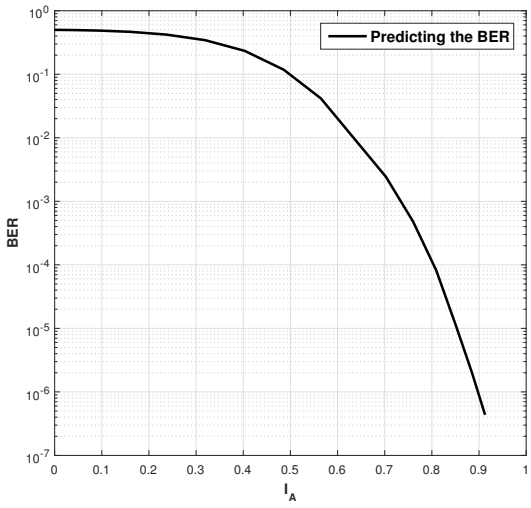

Figure 14. BER process for the BICM-ID decoder transfer characteristics function.

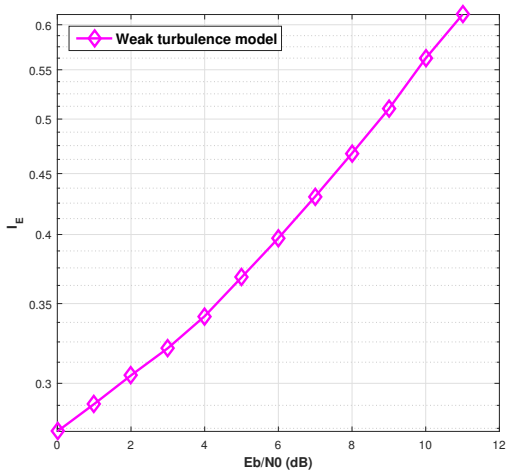

Figure 15. The impact of TWR-FSO with the PNC demapper over the weak turbulence link obtained by the Monte Carlo simulation.

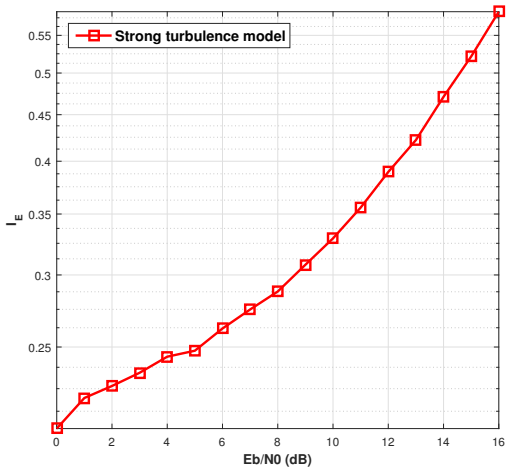

Figure 16. The impact of TWR-FSO with the PNC demapper over the strong turbulence link obtained by the Monte Carlo simulation.

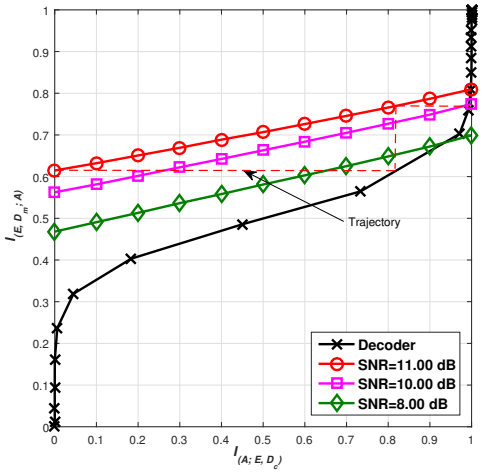

Figure 17. ExIT chart for the demapper E2E BICM-ID code with the PNC system employing the TWR-FSO weak link.

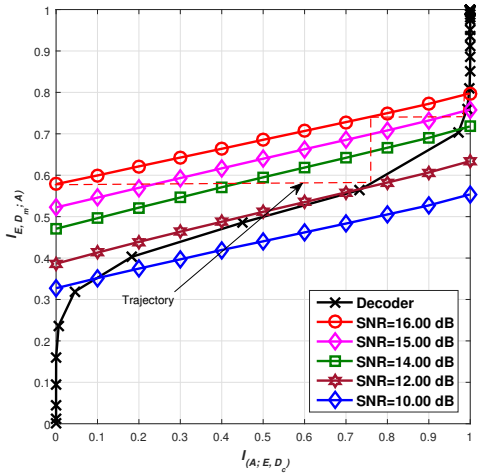

Figure 18. ExIT chart for the demapper E2E BICM-ID code with the PNC system employing the TWR-FSO strong link.

5. Conclusions

This paper outlined the implementation of an E2E BICM-ID code for a TWR-FSO PNC system operating over the distribution of light intensity fading due to atmospheric turbulence. We examined the bit error performance for the system under moderate to strong scenarios. Turbulence-induced channel fading was considered to describe large-scale and small-scale scintillations by log-normal and gamma-gamma distributions, respectively. Then, we investigated the decoding process of the system by using a graphical description; this involved implementing the technique of ExIT charts. ExIT charts allow the two concatenated codes in isolation of each other to aid the construction of good BICM iteratively-decoded code. Thus, the convergence occurs depending on the SNR in terms of E_b/N_0 with fewer iterations. Therefore, the start of the waterfall region can be known as the demapper affected by the corresponding value of SNR for the systems over log-normal and gamma-gamma distributions. The introduction of the results-based iterative decoding method had improved the performance of the TWR-FSO PNC system. The E2E performance of a BICM-ID code was evaluated on a TWR-FSO with PNC employed at the relay. This included the impact of a log-normal and a gamma-gamma distributions channel and then compared through simulation with a non-iterative convolutional code TWR-FSO PNC and uncoded TWR-FSO PNC systems. The simulation results along with the Monte Carlo simulation were matched to the exact analytical results of the ExIT charts.

Acknowledgments: First and second authors would like to gratefully acknowledge the financial support from Iraqi Ministry of Higher Education and Scientific Research for carrying out this research.

Conflicts of Interest: The authors declare no conflict of interest.

References

1. Ahlswede, R.; Cai, N.; Li, S.; Yeung, R. Network information flow. *IEEE Trans. Inf. Theory* **2000**, *46*, 1204–1216.
2. Zhang, S.; Liew, S.C.; Lam, P.P. Hot topic: physical layer network coding. In Proceedings of the 12th Annual International Conference on Mobile Computing and Networking (MobiCom), Los Angeles, CA, USA, 24–29 September 2006; pp. 358–365.
3. Andrews, L.C.; Phillips, R.L. *Laser Beam Propagation through Random Media*, 2nd ed.; SPIE: Bellingham, WA, USA, 2005; Volume PM152.
4. Ansari, I.S.; Abdallah, M.M.; Alouini, M.S.; Qaraqe, K.A. Outage performance analysis of underlay cognitive RF and FSO wireless channels. In Proceedings of the 3rd International Workshop in Optical Wireless Communications (IWOW), Madeira Island, Portugal, 17 September 2014; pp. 6–10,
5. Sandalidis, H.G. Coded free-space optical links over strong turbulence and misalignment fading channels. *IEEE Trans. Commun.* **2011**, *59*, 669–674.
6. Lee, I.E.; Ghassemlooy, Z.; Ng, W.P.; Uysal, M. Performance analysis of free space optical links over turbulence and misalignment induced fading channels. In Proceedings of the 8th International Symposium on Communication Systems, Networks & Digital Signal Processing (CSNDSP), Poznan, Poland, 18–20 July 2012; pp. 1–6.
7. Awan, M.S.; Brandl, P.; Leitgeb, E.; Nadeem, F.; Csugai-Horvath, L.; Nebuloni, R. Transmission of high data rate optical signals in fog and snow conditions. In Proceedings of the 1st International Conference on Wireless Communication, Vehicular Technology, Information Theory and Aerospace & Electronic Systems Technology, Aalborg, Denmark, 17–20 May 2009; pp. 702–706.
8. Hranilovic, S. Trends and progress in optical wireless communications. In Proceedings of the Optical Fiber Communications Conference and Exhibition (OFC), Los Angeles, CA, USA, 19–23 March 2017; pp. 1–3.
9. Chatzidiamantis, N.D.; Michalopoulos, D.S.; Kriezis, E.E.; Karagiannidis, G.K.; Schober, R. Relay selection protocols for relay-assisted free-space optical systems. *IEEE/OSA J. Opt. Commun. Netw.* **2013**, *5*, 92–103.
10. Karimi, M.; Nasiri-Kenari, M. Free space optical communications via optical amplify-and-forward relaying. *J. Lightwave Technol.* **2011**, *29*, 242–248.
11. Bhatnagar, M.R. Average BER analysis of differential modulation in DF cooperative communication system over gamma-gamma fading FSO links. *IEEE Commun. Lett.* **2012**, *16*, 1228–1231.
12. Zhou, X.; Zhang, D.; Yang, Y.; Obaidat, M.S. Network coded multiple source cooperation aided relaying for free space optical transmission. *Int. J. Commun. Syst.* **2012**, *25*, 1465–1478.
13. Zlatanov, N.; Hranilovic, D.; Evans, J.S. Buffer-Aided Relaying Improves Throughput of Full-Duplex Relay Networks With Fixed-Rate Transmissions. *IEEE Commun. Lett.* **2016**, *20*, 2446–2449.
14. Abu-Almaalie, Z.; Ghassemlooy, Z.; Le-Minh, H.; Aslam, N. Physical layer network coding with two-way relay free space optical communication link. In Proceedings of the Internet Technologies and Applications (ITA), Wrexham, UK, 8–11 September 2015; pp. 292–297.
15. Henniger, H.; Epple, B.; Giggenbach, D. Mobil FSO Activities in Europe and Fading Mitigation Approaches. In Proceedings of the 17th International Conference Radioelektronika, Brno, Czech Republic, 24–25 April 2007; pp. 1–6.
16. Almaalie, Z.A.; Ghassemlooy, Z.; Al-Rubaie, A.A.S.; Lee, I.E.; Le-Minh, H. Forward error correction with physical layer network coding in two-way relay free space optical links. In Proceedings of the 8th Computer Science and Electronic Engineering (CEEC), Colchester, UK, 28–30 September 2016; pp. 1–5.
17. Kumar, K.; Borah, D.K. Hybrid symbols for parallel optical/RF channels using BICM-ID. *Electron. Lett.* **2011**, *47*, 1189–1190.
18. Kumar, K.; Borah, D.K. Hybrid FSO/RF symbol mappings: Merging high speed FSO with low speed RF through BICM-ID. In Proceedings of the IEEE in Global Communications Conference (GLOBECOM), Anaheim, CA, USA, 3–7 December 2012; pp. 2941–2946.
19. Li, X.; Ritcey, J.A. Bit-interleaved coded modulation with iterative decoding. *IEEE Commun. Lett.* **1997**, *1*, 169–171.

20. Brink, S.T. Convergence of iterative decoding. *Electron. Lett.* **1999**, *35*, 806–808.
21. Farid, A.A.; Hranilovic, S. Outage capacity optimization for free-space optical links with pointing errors. *J. Lightwave Technol.* **2007**, *25*, 1702–1710.
22. Karp, R.M. *Optical Communications*, 2nd ed.; John Wiley: New York, NY, USA, 1995.
23. Zambrana, A.G.; Vázquez, C.C.; Vázquez, B.C. Outage performance of MIMO FSO links over strong turbulence and misalignment fading channels. *Opt. Express* **2011**, *19*, 13480–13496.
24. Zdravkovic, N.; Petkovic, M.I.; Djordjevic, G.T.; Kansanen, K. Outage analysis of mixed FSO/WiMAX link. *IEEE Photonics J.* **2016**, *8*, 1–14.
25. Proakis, J.G. *Digital Communications*, 4th ed.; McGraw Hill: New York, NY, USA, 2001.
26. Billingsley, P. *Probability and Measure*, 3rd ed.; John Wiley & Sons: Hoboken, NJ, USA, 1995.
27. Brink, S.T. Convergence behavior of iteratively decoded parallel concatenated codes. *IEEE Trans. Commun.* **2001**, *49*, 1727–1737.
28. Tuchler, M.; Hagenauer, J. EXIT charts of irregular codes. In Proceedings of the 36th Annual Conference on Information Sciences and Systems (CISS), Princton, NJ, USA, 21–23 March 2002; pp. 748–753.
29. Richardson, T.J.; Shokrollahi, M.A.; Urbanke, R.L. Design of capacity-approaching irregular low-density parity-check codes. *IEEE Trans. Inf. Theory* **2001**, *47*, 619–637.
30. Olmos, J.; Ruiz, S.; Lozano, M.G.; Sacristan, D.M. Link Abstraction Models Based on Mutual Information for LTE Downlink. Available online: https://goo.gl/46Hvm8 (accessed on 19 July 2017).
31. Brannstrom, F.; Rasmussen, L.K.; Grant, A.J. Convergence analysis and optimal scheduling for multiple concatenated codes. *IEEE Trans. Inf. Theory* **2005**, *51*, 3354–3364.